Entangled microwaves as a resource for entangling spatially separate solid-state qubits: Superconducting qubits, nitrogen-vacancy centers, and magnetic molecules

Angela Viviana Gómez,[1,2,*] Ferney Javier Rodríguez,[1] Luis Quiroga,[1] and Juan José García-Ripoll[2]
[1]*Departamento de Física, Universidad de Los Andes, Apartado Aéreo 4976, Bogotá, Distrito Capital, Colombia*
[2]*Instituto de Física Fundamental, IFF-CSIC, Calle Serrano 113b, Madrid E-28006, Spain*
(Received 1 December 2015; published 27 June 2016)

Quantum correlations present in a broadband two-line squeezed microwave state can induce entanglement in a spatially separated bipartite system consisting of either two single qubits or two-qubit ensembles. By using an appropriate master equation for a bipartite quantum system in contact with two separate but entangled baths, the generating entanglement process in spatially separated quantum systems is thoroughly characterized. Decoherence thermal effects on the entanglement transfer are also discussed. Our results provide evidence that this entanglement transfer by dissipation is feasible, yielding to a steady-state amount of entanglement in the bipartite quantum system which can be optimized for a wide range of realistic physical systems that include state-of-the-art experiments with nitrogen-vacancy centers in diamond, superconducting qubits, or even magnetic molecules embedded in a crystalline matrix.

DOI: 10.1103/PhysRevA.93.062336

I. INTRODUCTION

The generation and preservation of entanglement is one of the basic ingredients in many scalable quantum information protocols. Quantum cryptography [1,2], quantum communication [3], quantum repeaters, and certain models of quantum computation [4–6] demand preexisting entangled states, either at short distances or at long separations. If we focus on the establishment of pairwise entanglement, there exist three basic approaches: (i) an interaction in some past moment [7], (ii) a joint measurement with an entangled state as an outcome [8], or (iii) an interaction with a third party or mediator, such as phonons [9] or photons [10–13], which often can be reinterpreted as (ii) once the mediator is traced out.

We have cited some examples of atomic and molecular physics experiments where all these ideas have been put into practice. However, in recent years the field of solid-state quantum information processing has reached a status in which many of those entanglement protocols can be competitively reproduced, with similar goals and rapidly improving performance, using semiconductor quantum dots [14], nitrogen vacancy (NV) centers in diamond [15–17], superconducting qubits [18–20], surface plasmon polaritons [21], or superconducting microwave photons [22–26], to name a few possibilities. In this context, a remarkable idea is the hybridization of different technologies in a single setup, thus synthesizing the best of each. One attractive example is the integration of superconducting resonators with NV centers in diamond. These systems exploit the long coherence times of the NV spin in diamond jointly with the promise of high scalability and robust control of SC circuits [27–30]. Experimentally, the strong coupling between a spin ensemble and a superconducting resonator has been demonstrated in the linear or Gaussian regime [31–33], where the resonator and spin ensemble are both modeled as interacting harmonic oscillators. In addition, the strong coupling in this hybrid systems has made it possible to transfer the state between the NV ensemble and a superconducting resonator [34] while some other works show an improvement in the coherence times and the transfer of single excitations with a flux qubit [35].

A wealth of studies have clarified the transfer of entanglement from infinite-dimensional field systems to discrete matter systems, especially those involving driven cavities with embedded qubits [36,37]. A first proposal was limited to considering the unitary evolution of a separate microcavity plus a single qubit, with the radiation fields in a highly squeezed pure state [38]. Shortly afterwards, a highlighted scenario where two remote single-mode cavities containing a single qubit each was proposed to reach maximally entangled two-qubit states in both transient and steady-state regimes [39] by driving the cavities with highly entangled broadband two-mode Gaussian fields which act as local environments for each qubit. A standard formalism of second-order perturbation theory (Born-Markov approximation) makes it possible to determine the sufficient and necessary conditions to reach a successful entanglement transfer from a highly mixed but entangled broadband multimode reservoir to a spatially separate qubit pair [40]. Finally, pure and mixed entangled fields have also been proposed to quantum correlate pairs of other initially uncorrelated subsystems [41], especially when a mechanism for the replication over many matter subsystem pairs can be identified [42]. All of these protocols for the controlled manipulation of the entanglement distribution represent important steps towards the engineering of quantum networks. Motivated by this joint progress from both the theoretical and the experimental advances, in this work we study the transfer of entanglement from a continuous, broadband, two-line squeezed microwave field (TLSMF) as generated by Josephson parametric amplifiers (JPAs) [43], onto a bipartite system consisting of two qubits or two spin ensembles—either which can be made of NV centers, molecular magnets [44], or superconducting qubits—roughly as sketched in Fig. 1. By contrast with previously described protocols, here we propose a new scheme for gene-rating entanglement between spatially remote qubit systems exploiting a setup which accommodates

*av.gomez176@uniandes.edu.co

 ©2016 American Physical Society

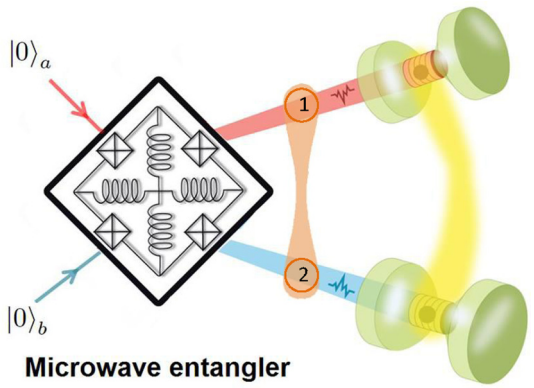

FIG. 1. System. Two spatially separated qubits (or two-qubit ensembles) in different branches coupled with entangled microwaves generated by a parametric Josephson amplifier.

the peculiarities of circuit-QED and of the novel field of propagating quantum microwaves, without resorting to embed the qubits in a microcavity but leaving them to couple directly with the TLSMF which is being continuously replenished. Moreover, we allow the qubit subsystems to be in contact with local environments which provide fully incoherent processes (thermal decoherence) which compete with the quantum coherent generating processes as represented by the TLSMF. In this way, we provide quantitative evidence for limitations on the entanglement transfer as caused by ubiquitous thermal events, a shortcoming of previous studies [39,40]. We thus study the pure TLSMF entanglement transfer power as well as its limitations set by additional couplings to thermal baths, extending earlier results for quantum systems in contact with several bath fields [45,46], using Markovian master equations.

The paper is organized as follows. Section II describes the general formalism for addressing the entanglement driving by two dissipative entangled baths as represented by TLSMF. The case of a matter subsystem corresponding to two single separate qubits is developed in Sec. III, while Sec. IV is devoted to two distant qubit ensembles. The solutions discussed in those sections encompass both resonant and nonresonant cases between central microwave frequency and matter. Further decoherence effects on the qubit pair or qubit ensembles are considered in Sec. V. Realistic solid-state implementations are explored in Sec. VI, where experimental parameters appropriate to NV centers in diamond, superconducting qubits, and magnetic molecules are considered. Finally, Sec. VII summarizes our main conclusions, while technical details are relegated to the appendixes.

II. BIPARTITE QUANTUM SYSTEM IN CONTACT WITH TWO SEPARATE BATHS

We start by putting on theoretical ground the formalism yielding to the master equation describing the generation of quantum correlations on a quantum matter bipartite system by driving from two separate entangled (microwave) reservoirs. In this section we limit ourselves to the effects of the TLSMF on the matter subsystem. Other couplings of the matter with additional reservoirs providing extra matter decoherence channels are discussed below; see Sec. V. Here we follow and extend to squeezed reservoirs previous results from [45,46], which have been already applied to a quantum system coupled to two thermal reservoirs at different temperatures. We consider a composed quantum system, including the baths, formed by two spatially separated lines or branches, as depicted in Fig. 1. In each branch a part of a multisqueezed microwave field interacts locally with a quantum system of interest. Thus, the full Hamiltonian reads as

$$\hat{H} = \sum_{j=1}^{2} \hat{H}_j = \sum_{j=1}^{2} (\hat{Q}_j + \hat{R}_j + \hat{V}_j), \tag{1}$$

where for arm j, $\hat{Q}_j$, $\hat{R}_j$, and $\hat{V}_j$ denote the partial Hamiltonians for the quantum or matter system itself, the free microwave radiation field, and the matter-radiation interaction terms, respectively. Notice that $[\hat{H}_1, \hat{H}_2] = 0$.

The aim is to find the equation of motion for the quantum system reduced density operator, $\hat{\rho}(t)$, from the unitary evolution of the full supersystem density operator $\hat{\gamma}(t)$. To proceed further we express the full dynamics in the interaction picture given by the transformation

$$\hat{U}^{\dagger}(t) = \hat{U}_1^{\dagger}(t)\hat{U}_2^{\dagger}(t) = \prod_{j=1}^{2} e^{i(\hat{Q}_j + \hat{R}_j)t}, \tag{2}$$

such that an interaction picture operator $\hat{O}_I(t)$ is connected with its Schrödinger version $\hat{O}_S$ by $\hat{O}_I(t) = \hat{U}^{\dagger}(t)\hat{O}_S\hat{U}(t)$. The full supersystem (bipartite quantum system + reservoirs) density operator satisfies the Liouville-Von Neumann equation ($\hbar = 1$)

$$\frac{d\hat{\gamma}_I(t)}{dt} = -i[\hat{V}_I(t), \hat{\gamma}_I(t)], \tag{3}$$

with $\hat{V}_I(t) = \hat{V}_{1,I}(t) + \hat{V}_{2,I}(t)$. We assume that the coupling strength between the central quantum matter system and the microwave reservoirs is weak enough to express $\hat{\gamma}(t)$ as

$$\hat{\gamma}_I(t) = \hat{\rho}_I(t) \otimes \hat{\rho}_{1,2}^{B}, \tag{4}$$

where the baths are described by a stationary correlated (nonseparable) density matrix $\hat{\rho}_{1,2}^{B}$. Thus, up to second order in the matter-radiation interaction strength, we obtain [45,46]

$$\frac{d\hat{\rho}_I(t)}{dt} = (-i)^2 \int_0^t dt_1 \mathrm{Tr}_R\{[\hat{V}_I(t), [\hat{V}_I(t_1), \hat{\rho}_I(t_1) \otimes \hat{\rho}_{1,2}^{B}]]\}, \tag{5}$$

where $\mathrm{Tr}_R\{\cdots\}$ denotes the partial trace over the squeezed microwave radiation reservoirs.

According to [24] the broadband TLSMF produced by a JPA (see Fig. 1) can be described by $|S_q\rangle = \hat{S}|\{0\}_1\rangle \otimes |\{0\}_2\rangle$ [47], where the two-arm multimode vacuum state is denoted as $|\{0\}_1\rangle \otimes |\{0\}_2\rangle$, in such a way that the stationary entangled baths are described by a nonseparable density operator of the form

$$\hat{\rho}_{1,2}^{B} = \hat{S}|\{0\}_1\rangle \otimes |\{0\}_2\rangle\langle\{0\}_2| \otimes \langle\{0\}_1|\hat{S}^{\dagger}, \tag{6}$$

indicating that in the arm j a broadband multimode distribution centered on frequency ω_{Lj} is found. The multimode squeezing

operator is given by

$$\hat{S} = \exp\left\{\sum_{n,m} s(\omega_n,\omega_m)[\hat{a}_1^\dagger(\omega_{L1}+\omega_n)\hat{a}_2^\dagger(\omega_{L2}-\omega_m) - \hat{a}_1(\omega_{L1}+\omega_n)\hat{a}_2(\omega_{L2}-\omega_m)]\right\}, \quad (7)$$

where $\hat{a}_1(\omega_{L1}+\omega_n)$ and $\hat{a}_2(\omega_{L2}-\omega_n)$ denote the photon annihilation operators for mode n of arms $j=1,2$, respectively. Although microwaves over a broadband continuum of modes are assumed, the mode indexes n,m in Eq. (7) are represented by discrete labels for simplicity. In Eq. (7), $s(\omega_n,\omega_m)=s_{n,m}$ are associated with the function (taken as real) of squeezing parameters between mode $\omega_{L1}+\omega_n$ in path 1 and mode $\omega_{L2}-\omega_m$ in path 2. The multimode entangled state given by Eq. (6) describes two spatially separated but highly *entangled baths* that we use as a resource for entangling the matter subsystems themselves.

The microwave reservoirs are described by local Hamiltonians in each arm such as

$$\hat{R} = \sum_{j=1}^{2}\hat{R}_j = \sum_{j=1}^{2}\sum_n[\omega_{Lj}-(-1)^j\omega_n]\hat{a}_{n,j}^\dagger\hat{a}_{n,j}. \quad (8)$$

In the last equation we have explicitly written $\hat{a}_{n,1}$ and $\hat{a}_{n,2}$ in place of $\hat{a}_1(\omega_{L1}+\omega_n)$ and $\hat{a}_2(\omega_{L2}-\omega_n)$, respectively, a double notation that we take as equivalent in the following. Additionally, the matter Hamiltonian can be written as

$$\hat{Q} = \sum_{j=1}^{2}\hat{Q}_j = \sum_{j=1}^{2}\omega_j\hat{q}_j^+\hat{q}_j^-, \quad (9)$$

where $\hat{q}_j^\pm$ denote single excitation operators for the matter subsystem in branch j and the commutation relation $[\hat{q}_j^+\hat{q}_j^-,\hat{q}_{j'}^\pm]=\pm\hat{q}_j^\pm\delta_{j,j'}$ should hold. The specific physical meaning of ω_j and $\hat{q}_j^\pm$ in Eq. (9) are discussed below for different cases. Finally, the matter-radiation interaction term in arm j becomes

$$\hat{V} = \sum_{j=1}^{2}\hat{V}_j = \sum_{j=1}^{2}\sum_n g_{n,j}(\hat{q}_j^+\hat{a}_{n,j}+\hat{q}_j^-\hat{a}_{n,j}^\dagger), \quad (10)$$

where $g_{n,j}=g_j[\omega_{Lj}-(-1)^j\omega_n]$ is the coupling strength between matter subsystem and mode n in branch j. Therefore, the interaction picture expression for the matter-radiation coupling Hamiltonian takes the form

$$\begin{aligned}\hat{V}_I(t) = &\sum_n g_1(\omega_{L1}+\omega_n)(\hat{q}_1^+\hat{a}_{n,1}e^{i(\omega_1-\omega_{L1}-\omega_n)t} \\ &+\hat{q}_1^-\hat{a}_{n,1}^\dagger e^{-i(\omega_1-\omega_{L1}-\omega_n)t}) \\ &+\sum_n g_2(\omega_{L2}-\omega_n)(\hat{q}_2^+\hat{a}_{n,2}e^{i(\omega_2-\omega_{L2}+\omega_n)t} \\ &+\hat{q}_2^-\hat{a}_{n,2}^\dagger e^{-i(\omega_2-\omega_{L2}+\omega_n)t}). \end{aligned} \quad (11)$$

By inserting Eq. (11) into Eq. (5), expressions involving bath operators such as $\mathrm{Tr}_{R_1,R_2}\{\hat{\rho}_{1,2}^B\hat{a}_{n,k}^\pm\hat{a}_{m,j}^\pm\}=\langle\hat{a}_{n,k}^\pm\,\hat{a}_{m,j}^\pm\rangle$ $(j,k=1,2)$ should be evaluated, which for the entangled bath density

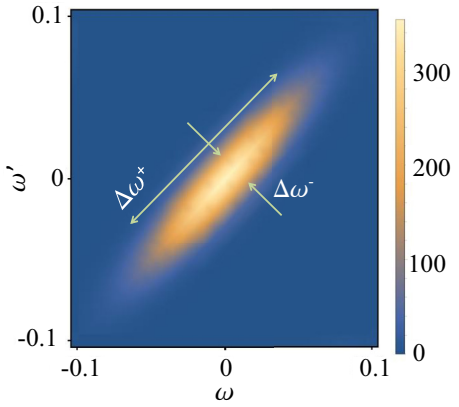

FIG. 2. Microwave squeezing strength $s(\omega,\omega')$ described by a double Gaussian function of two arm frequencies ω and ω' (in ω_L units, $\omega_{L1}=\omega_{L2}=\omega_L$) with $\Delta\omega^+=0.09\omega_L$ and $\Delta\omega^-=0.02\omega_L$.

operator given by Eq. (6) leads to

$$\langle\hat{a}_{n,k}^\pm\,\hat{a}_{m,j}^\pm\rangle=(\langle\{0\}_1|\otimes\langle\{0\}_2|\,\hat{S}^\dagger\,\hat{a}_{n,k}^\pm\,\hat{a}_{m,j}^\pm\,\hat{S}\,|\{0\}_1\rangle\otimes|\{0\}_2\rangle. \quad (12)$$

The squeezing function $s_{n,m}$ in Eq. (7) is assumed to be Gaussian [48], i.e.,

$$s_{n,m}=\tilde{s}\left(\frac{2}{\pi\,\Delta\omega^-\Delta\omega^+}\right)e^{-(\frac{\omega_n-\omega_m}{\Delta\omega^-})^2}e^{-(\frac{\omega_n+\omega_m}{\Delta\omega^+})^2}, \quad (13)$$

where $\Delta\omega^-$ is associated with the width of the two-bath correlations as determined by the JPA pump duration, while $\Delta\omega^+$ corresponds to the spectral width of the two arms coherence (see Fig. 2). A special situation occurs when the two-bath correlations are perfect, i.e., $\Delta\omega^-\to 0$, transforming the first Gaussian in Eq. (13) in a δ function, yielding to $s_{n,m}=\delta_{n,m}s_n$ with

$$s_n = s_0 e^{-(\frac{2\omega_n}{\Delta\omega^+})^2} \quad (14)$$

being s_0 the maximum squeezing between microwaves at central frequencies ω_{L1} and ω_{L2}. The reservoir correlations are then given by the expressions (see the Appendix)

$$\begin{aligned}\langle\hat{a}_{n,1}^\dagger\hat{a}_{m,1}\rangle &= \langle\hat{a}_{n,2}^\dagger\hat{a}_{m,2}\rangle=\delta_{n,m}\sinh^2(r_n), \\ \langle\hat{a}_{n,1}^\dagger\hat{a}_{m,2}^\dagger\rangle &= \langle\hat{a}_{n,1}\hat{a}_{m,2}\rangle=\delta_{n,m}\sinh(r_n)\cosh(r_n), \\ \langle\hat{a}_{n,1}\hat{a}_{m,1}^\dagger\rangle &= \langle\hat{a}_{n,2}\hat{a}_{m,2}^\dagger\rangle=\delta_{n,m}\cosh^2(r_n). \end{aligned} \quad (15)$$

In the following, we assume that the frequency detunings $(\Delta_j=\omega_j-\omega_{Lj})$ between quantum matter (ω_j) and central microwave distribution (ω_{Lj}) satisfy the condition $\Delta_1=-\Delta_2=\Delta$, although nonspecific relation between ω_1 and ω_2 is required. Arbitrary detuning effects are discussed elsewhere. Within the Wigner-Weisskopf approach, Eq. (5) yields to a master equation in Lindblad form as

$$\frac{d\hat{\rho}}{dt}=\hat{\mathcal{L}}_{MW}\hat{\rho}(t)=[\hat{\mathcal{L}}_1+\hat{\mathcal{L}}_2+\hat{\mathcal{L}}_{1,2}]\hat{\rho}(t), \quad (16)$$

where the MW label in the Lindbladian $\hat{\mathcal{L}}_{MW}$ reinforces the idea of just taking into account TLSMF effects for the moment.

The *local* TLSMF terms are given by ($j = 1,2$)

$$\hat{\mathcal{L}}_j\hat{\rho}(t) = \Gamma_j(\Delta)\{\cosh^2[s(\Delta)][2\hat{q}_j^-\hat{\rho}(t)\hat{q}_j^+ - \hat{q}_j^+\hat{q}_j^-\hat{\rho}(t) - \hat{\rho}(t)\hat{q}_j^+\hat{q}_j^-] + \sinh^2[s(\Delta)][2\hat{q}_j^+\hat{\rho}(t)\hat{q}_j^- - \hat{q}_j^-\hat{q}_j^+\hat{\rho}(t) - \hat{\rho}(t)\hat{q}_j^-\hat{q}_j^+]\}, \quad (17)$$

where, according to Eq. (14), $s(\Delta) = s_0 e^{-(\frac{2\Delta}{\Delta\omega^+})^2}$, and the effective *local* matter-radiation coupling becomes given by

$$\Gamma_j(\Delta) = \sum_n |g_j[\omega_{Lj} - (-1)^j\omega_n]|^2\delta(\omega_n - \Delta). \quad (18)$$

Furthermore, the cross or *nonlocal* TLSMF Lindblad term in Eq. (16) reads as

$$\hat{\mathcal{L}}_{1,2}\hat{\rho}(t) = \Gamma_{1,2}(\Delta)\sinh[2s(\Delta)]\{[2\hat{q}_2^+\hat{\rho}(t)\hat{q}_1^+ - \hat{\rho}(t)\hat{q}_1^+\hat{q}_2^+ - \hat{q}_1^+\hat{q}_2^+\hat{\rho}(t)] + [2\hat{q}_1^+\hat{\rho}(t)\hat{q}_2^+ - \hat{\rho}(t)\hat{q}_2^+\hat{q}_1^+ - \hat{q}_2^+\hat{q}_1^+\hat{\rho}(t)] + \text{H.c.}\}, \quad (19)$$

where the effective *nonlocal* matter-bath coupling constant in Eq. (19) is given by

$$\Gamma_{1,2}(\Delta) = \sum_n g_1(\omega_{L1} + \omega_n)g_2(\omega_{L2} - \omega_n)\delta(\omega_n - \Delta) \quad (20)$$

and H.c. denotes the Hermitian conjugate terms. Lindblad terms such as $\hat{\mathcal{L}}_j$ in Eq. (17) denote the dissipative coupling of microwaves in line j with its respective matter subsystem. These local dissipative terms have similar forms as the coupling of a single matter piece with a single thermal bath, thus producing a null result for entanglement. Indeed, the most interesting dissipative term is the nonlocal Lindblad term $\hat{\mathcal{L}}_{1,2}$ in Eq. (19), which is the responsible for entangling the two matter subsystems. In the next two sections we apply this formalism to different physical systems, specifically those formed by two individual separate qubits, as well as to different ensembles of qubits interacting with entangled microwave photons.

III. BIPARTITE QUANTUM SYSTEM: A SOLID-STATE QUBIT PAIR

The first setup under consideration is a hybrid combination of two separate single qubits, interacting with a broadband TLSMF. The solid-state qubits could be individual NV centers, magnetic nanomolecules or superconducting qubits, while the entangled microwave fields can be generated in a variety of ways from JPA devices. The qubits are represented by Pauli operators $\hat{\sigma}_{j,z}$ and $\hat{\sigma}_j^{\pm}$, with splitting energies ω_j ($j = 1,2$). The qubit-radiation interaction strength is given by $g_{n,j} = g_j[\omega_{Lj} - (-1)^j\omega_n]$ for the qubit in the transmission line j coupled to mode n. In order to quantify the entangling power of the microwave entangled reservoirs acting on the noninteracting qubit pair, we start by writing down solutions to the master equation given in Eq. (16) with Lindblad terms as in Eqs. (17) and (19), with the substitutions $\hat{q}_j^+ \to \hat{\sigma}_j^+$ and $\hat{q}_j^- \to \hat{\sigma}_j^-$. The effect of the squeezing between the baths on the qubit pair evolution is evident in the crossed Lindblad term $\hat{\mathcal{L}}_{1,2}$, where the presence of simultaneous two-qubit excitation operators $\hat{\sigma}_1^+$ and $\hat{\sigma}_2^+$ (or their Hermitian conjugates) occurs. In a two-qubit base ordered as $\{|+,+\rangle, |+,-\rangle, |-,+\rangle, |-,-\rangle\}$ the two-qubit density operator $\hat{\rho}(t)$ has the form

$$\hat{\rho}(t) = \begin{pmatrix} \rho_{1,1}(t) & 0 & 0 & \rho_{1,4}(t) \\ 0 & \rho_{2,2}(t) & 0 & 0 \\ 0 & 0 & \rho_{3,3}(t) & 0 \\ \rho_{4,1}(t) & 0 & 0 & \rho_{4,4}(t) \end{pmatrix}, \quad (21)$$

which is very convenient to evaluate entanglement measures such as the logarithmic negativity or concurrence [49,50]. Though for a qubit pair these two measures are equivalent, in this paper we focus on the concurrence (C). The initial two-qubit density operator corresponds to $\hat{\rho}(0) = |-,-\rangle\langle-,-|$; i.e., the qubit pair is in its ground state. We have solved analytically the master equation for the qubits in the stationary regimen and evaluated consequently the concurrence.

The stationary solution for the density matrix $\hat{\rho}^{ss}$ can be found analytically, which for the density matrix given in Eq. (21), yields $\rho_{2,2}^{ss} = \rho_{3,3}^{ss}$ and

$$C^{ss} = 2\text{Max}\{0, |\rho_{1,4}^{ss}| - \rho_{2,2}^{ss}\} = \text{Max}\left\{0, \frac{2\gamma\tanh[2s(\Delta)] - (\gamma^2-1)\sinh^2[2s(\Delta)]}{(\gamma^2+1) + (\gamma^2-1)\cosh[4s(\Delta)]}\right\}, \quad (22)$$

where $\gamma = (\gamma_1 + \gamma_2)/2$, with $\gamma_j = \Gamma_j/\Gamma$ (from now on we shall simply denote $\Gamma = \Gamma_{1,2}$). Note that the steady-state two-qubit reduced density matrix, and consequently C^{ss}, does not depend separately on the individual dissipation rates γ_j but only on their average value γ. Additionally, it is straightforward to verify that by putting $s_0 = 0$ in Eq. (22), i.e., nonsqueezed microwave baths, each qubit is directly coupled to a local vacuum or zero-temperature reservoir with no crossed arm couplings, producing a long-time diagonal density operator with $\rho_{1,1}^{ss} = \rho_{2,2}^{ss} = \rho_{3,3}^{ss} = \rho_{1,4}^{ss} = 0$ and $\rho_{4,4}^{ss} = 1$, corresponding to a vanishing qubit pair entanglement, $C^{ss} = 0$.

The result expressed by Eq. (22) holds whenever $\gamma \geqslant 1$; otherwise, the Lindblad master equation given by the set of Eqs. (16), (17) and (19) does not possess steady-state solutions. The simplicity of this result allows us to obtain an analytical expression for the borderline in the parameter plane $[\gamma, s(\Delta)]$,

$$\sinh[4s(\Delta)] = \frac{4\gamma}{\gamma^2 - 1}, \quad (23)$$

as shown by the yellow line in Fig. 3(a), separating regions of zero steady-state concurrence from regions of finite steady-state entanglement. As depicted in Fig. 3(a), if the microwave squeezing parameter $s(\Delta)$ increases, the steady-state concurrence is also increased, but in order to reach this steady-state value, a longer time is required. For the special case $\gamma = 1$, i.e., identical local average and nonlocal cross-dissipation rates, we found $C^{ss} = \tanh[2s(\Delta)]$, indicating that for a near resonance condition, $\Delta \approx 0$, and large microwave squeezing, $r \gg 1$, the stationary concurrence gets saturated to its maximum value, $C^{ss} \to 1$, which corresponds to the qubit pair state approaching the pure Bell state $|\Psi^{ss}\rangle \approx \frac{1}{\sqrt{2}}(|+,+\rangle - |-,-\rangle)$.

The two-qubit concurrence time evolution, $C(t)$, is depicted in Fig. 3(b) for some selected values of the squeezing parameter $s(\Delta)$ and local dissipation γ terms, as marked by symbols in Fig. 3(a). Although the precise time evolution of $C(t)$ does depend on the individual values of γ_j, from now

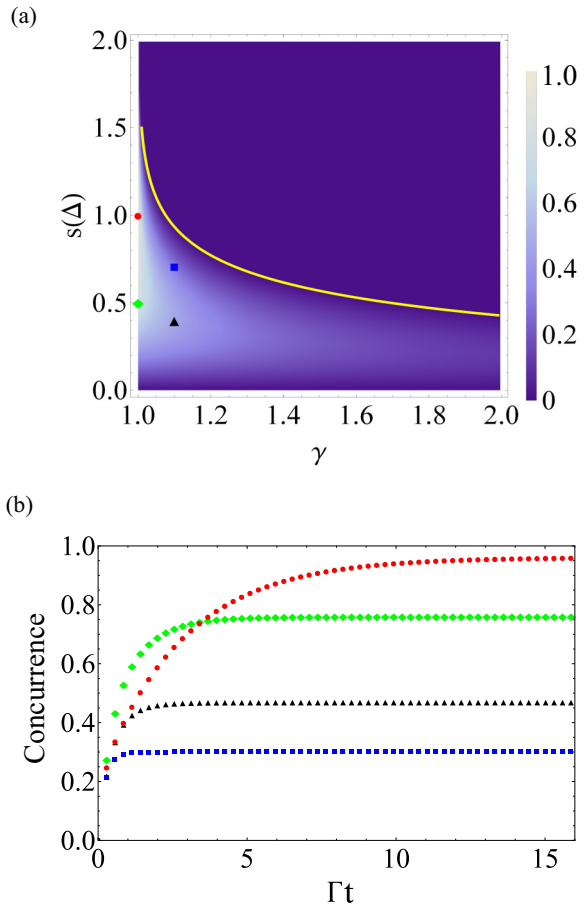

FIG. 3. Two-qubit concurrence C. (a) Steady-state C^{ss} as a function of the microwave squeezing parameter $s(\Delta)$ and $\gamma = (\gamma_1 + \gamma_2)/2$; the solid (yellow) line corresponds to Eq. (23). (b) Time-dependent $C(t)$ for selected parameters as marked by similar symbols in (a) for two initially unentangled qubits.

on we restrict ourselves to illustrating results only for the symmetric case, i.e., $\gamma_1 = \gamma_2$. In all cases the concurrence starts growing linearly in time, i.e., $C(t) \sim t$, at short times. For the special line $\gamma = 1$ in Fig. 3(a) the steady-state concurrence value, C^{ss}, requires longer times to be reached as the squeezing parameter $s(\Delta)$ gets larger.

Next we discuss the two-qubit entanglement generation process from an unentangled initial two-qubit state, by considering separately the effects of the microwave resonance squeezing strength s_0 and the detuning between central microwave frequency and qubit splitting, Δ. In Fig. 4(a), the steady-state concurrence C^{ss} for $\gamma = 1$ is plotted as a function of the resonance squeezing strength s_0 and the central microwave frequency-qubit detuning, Δ. The time dependence of $C(t)$ is shown in Fig. 4(b) for the zero-detuning case, i.e., $\Delta = 0$, as a function of the squeezing parameter s_0 [green points in Fig. 4(a)], while in Fig. 4(c) $C(t)$ is shown for the special microwave squeezing amount $s_0 = 1$ as a function of the detuning Δ [black points in Fig. 4(a)]. In Fig. 4(c) a two-time entanglement evolution is also evident: a fast entanglement generation at short times with $C(t) \sim t$ followed by a slower time evolution towards the saturation value, a clear behavior especially seen near resonance.

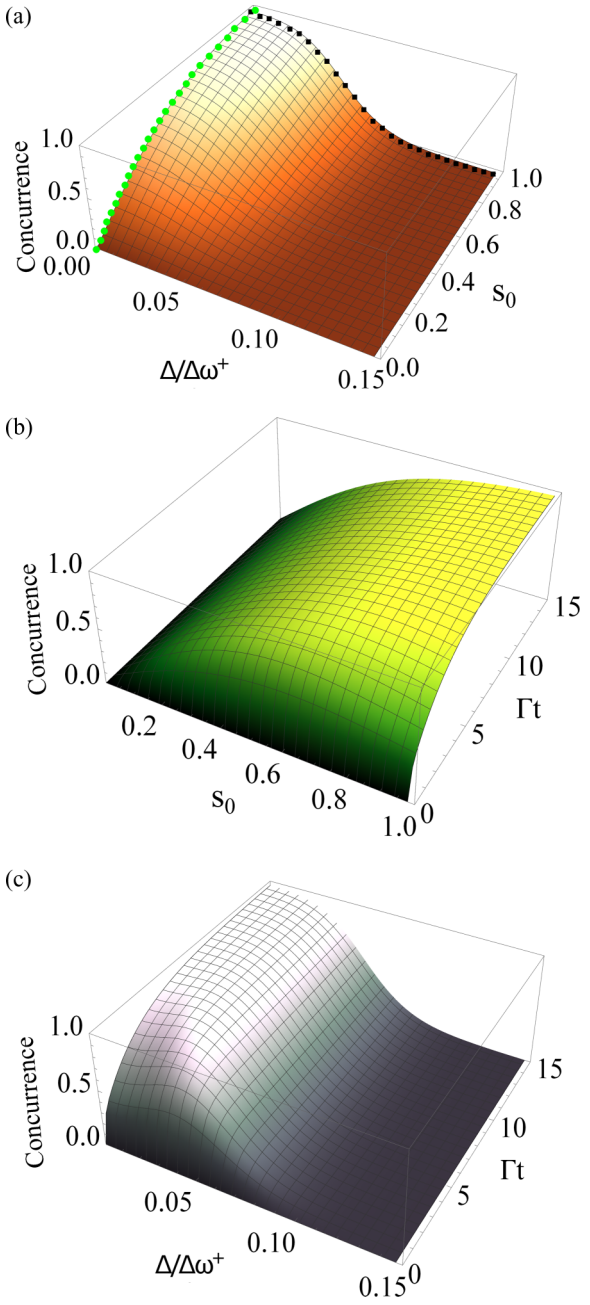

FIG. 4. Concurrence for two initially unentangled qubits for $\gamma = 1$. (a) Steady-state C^{ss} as a function of the resonance squeezing strength s_0 and the central microwave frequency-qubit detuning, Δ. (b) Time-dependent $C(t)$ at zero detuning, $\Delta = 0$ [green points in (a)]. (c) Time-dependent $C(t)$ at fixed maximum squeezing $s_0 = 1$ [black points in (a)].

In order to further explore the entanglement generation process, we now consider some points in the parameter space [see Fig. 3(a)] outside the special $\gamma = 1$ line. The two-qubit time-dependent concurrence $C(t)$ is depicted in Fig. 5 for symmetric local dissipation rates larger than the nonlocal or cross-dissipation rate, i.e., $\gamma = 1.1$. Figure 5(a) shows results of $C(t)$ at resonance $\Delta = 0$ as a function of the squeezing parameter s_0, where it is clear that $C(t)$ goes rapidly to its steady-state value for a microwave squeezing $s_0 \approx 0.5$.

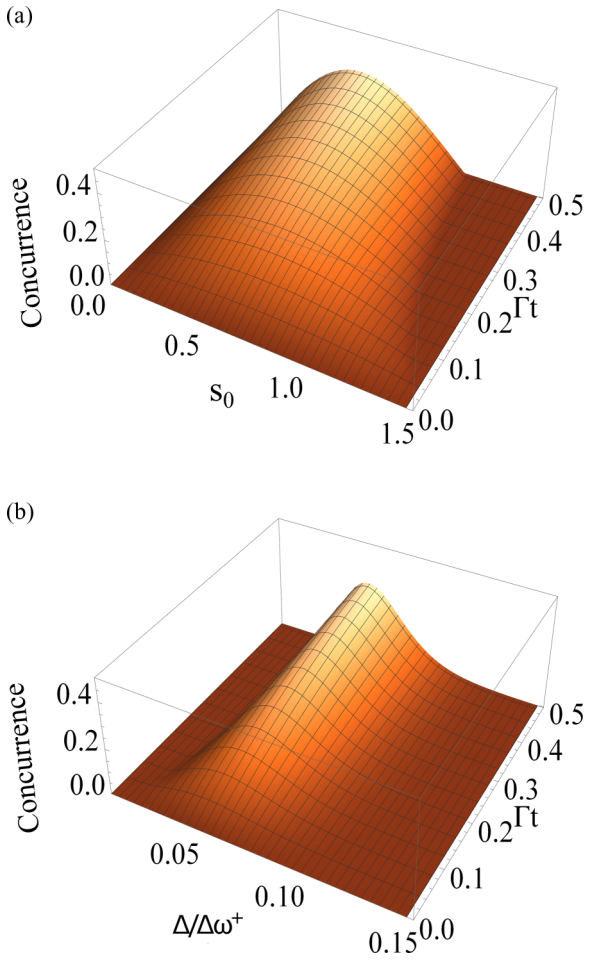

FIG. 5. Time-dependent two-qubit entanglement generation, $C(t)$, for initially unentangled qubits with symmetric local dissipation rates larger than the cross-dissipation rate, $\gamma = 1.1$. (a) Resonance, $\Delta = 0$; (b) fixed maximum squeezing parameter $s_0 = 1.5$.

However, at variance with the time evolution behavior for $\gamma = 1$ [see Fig. 4(b)] for which the larger s_0, the larger is the steady-state entanglement generation, now for $\gamma = 1.1$ there is only a transient generation of $C(t)$ with a vanishing steady-state limit, as shown in Fig. 3(a). An interesting behavior is uncovered by the plot in Fig. 5(b): By starting with a high microwave entanglement as corresponds to $s_0 = 1.5$ *and* the resonance condition $\Delta = 0$, the two-qubit concurrence remains stuck to zero [both transient and steady-state values vanish; see Fig. 3(a)]; however, by detuning the qubit-microwave interaction, i.e., letting $\Delta > 0$, the effective squeezing parameter decreases $s(\Delta) < s_0$, allowing for the generation of two-qubit entanglement, as can also been seen as a process where one starts at a point above the yellow line in Fig. 3(a) and, by varying enough the detuning, one crosses the yellow line to the zone of the parameter space where a steady-state entanglement is allowed. Thus, this behavior could mitigate the necessity of a special γ value to generate a finite two-qubit entanglement.

The crucial result of this section is that effectively it is possible to entangle distant qubits initially prepared in a separable state by using two entangled broadband microwave baths.

IV. BIPARTITE QUANTUM SYSTEM: TWO NONINTERACTING QUBIT ENSEMBLES

In the preceding section we showed that a finite amount of entanglement of two initially separated qubits can be generated from two highly correlated microwave baths. However, this transfer process is strongly limited by the coupling strength between the qubits and the microwave radiation. In order to increase the matter-radiation coupling, we propose to replace the system of two single qubits with two spin ensembles. In this way the matter-radiation coupling increases as $g \sim g_e\sqrt{N}$, where g_e is the coupling of a single qubit with the microwave photons, yielding to an absolute increase of both local and nonlocal dissipation rates Γ_j and Γ. An immediate positive consequence of this enhancement is to cut down the rise time of the entanglement generation to reach the steady-state final value for two spin ensembles.

Assuming that each spin ensemble has a low polarization, i.e., they remain close to its global ground state, we can introduce collective bosonic operators associated with each qubit ensemble $\hat{b}_j, \hat{b}_j^\dagger$, $j = 1,2$ [51]. Thus, now we consider a central quantum system formed by two independent single-mode boson fields, each of them coupled to a different reservoir of microwave radiation, but, as before, these microwave reservoirs still stay in a broadband squeezed multimode state. The master equation for the spin ensembles has the same structure as for single qubits, given by Eq. (16), with the Lindblad terms as given in Eqs. (17) and (19) but now with the replacements $\hat{q}_j^+ \to \hat{b}_j^\dagger$ and $\hat{q}_j^- \to \hat{b}_j$ $(j = 1,2)$.

We study the dynamics of a subsystem composed of two initially noninteracting spin ensembles coupled to a broadband TLSMF from a JPA. We are interested in the time evolution of the degree of entanglement of the spin ensembles, having initially zero excitations, i.e., $\hat{\rho}(0) = |0,0\rangle\langle 0,0|$, once they have interacted with the entangled microwaves. The state for the pair of spin ensembles is entirely specified by its covariance matrix, which is a real, symmetric, and positive matrix [49,52,53],

$$\hat{\sigma}(t) = \begin{pmatrix} \sigma_{xx} & \sigma_{xp_x} & \sigma_{xy} & \sigma_{xp_y} \\ \sigma_{xp_x} & \sigma_{p_xp_x} & \sigma_{yp_x} & \sigma_{p_xp_y} \\ \sigma_{xy} & \sigma_{yp_x} & \sigma_{yy} & \sigma_{yp_y} \\ \sigma_{xp_y} & \sigma_{p_xp_y} & \sigma_{yp_y} & \sigma_{p_yp_y} \end{pmatrix}. \tag{24}$$

The entries of the last matrix, $\sigma_{\alpha\beta}$, with $\alpha,\beta = x, y, p_x, p_y$, are given by

$$\sigma_{\alpha\beta} = \tfrac{1}{2}\langle\hat{\alpha}\hat{\beta} + \hat{\beta}\hat{\alpha}\rangle - \langle\hat{\alpha}\rangle\langle\hat{\beta}\rangle, \tag{25}$$

and they are computed from the canonical boson spin ensemble operators as

$$\hat{x}_j = \frac{(\hat{b}_j + \hat{b}_j^\dagger)}{\sqrt{2}}, \quad \hat{p}_j = \frac{(\hat{b}_j - \hat{b}_j^\dagger)}{i\sqrt{2}}, \tag{26}$$

with $(\hat{x}_1, \hat{p}_1) = (\hat{x}, \hat{p}_x)$ and $(\hat{x}_2, \hat{p}_2) = (\hat{y}, \hat{p}_y)$.

The entanglement of a two-mode Gaussian state is measured by the logarithmic negativity E_N, which has a closed

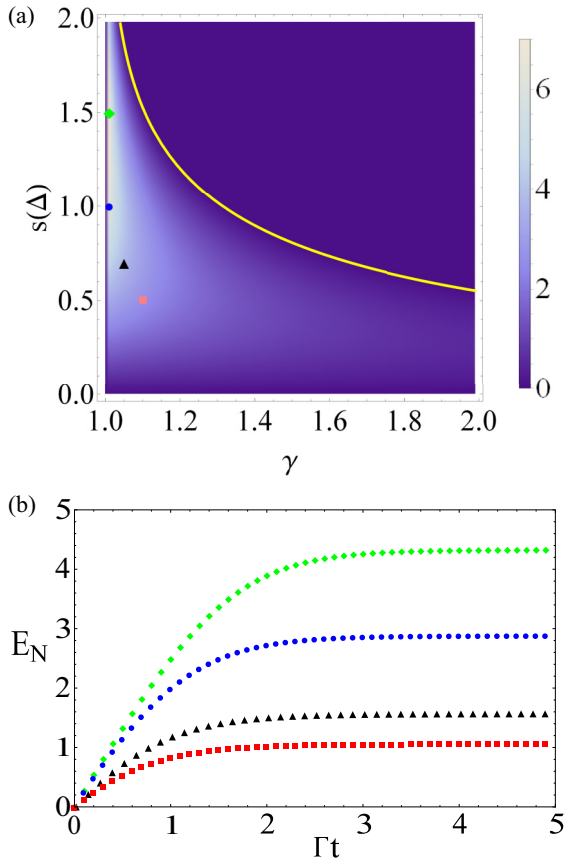

FIG. 6. Logarithmic negativity, E_N, for two spin ensembles. (a) Steady-state E_N^{ss} as a function of the microwave squeezing parameter $s(\Delta)$ and γ; the solid (yellow) line corresponds to Eq. (34). (b) Time-dependent $E_N(t)$ for selected parameters as marked by similar symbols in (a) for two initially unentangled spin ensembles.

expression given by

$$E_N = \mathrm{Max}\{0, -\log_2 2\tilde{\nu}_-\}. \tag{27}$$

Here $\tilde{\nu}_-$ represents the smallest of the two symplectic eigenvalues of the partial transpose $\tilde{\sigma}$ of the two-mode covariance matrix $\hat{\sigma}$. Writing the matrix $\hat{\sigma}$ in terms of 2×2 blocks,

$$\sigma \equiv \begin{pmatrix} \hat{A} & \hat{C} \\ \hat{C}^T & \hat{B} \end{pmatrix}, \tag{28}$$

the logarithmic negativity in Eq. (27) reads as

$$E_N(t) = \mathrm{Max}\left\{0, -\frac{1}{2}\log_2[4G(\sigma(t))]\right\}, \tag{29}$$

$$G(\sigma) = \frac{1}{2}(\det A + \det B) - \det C - \left\{\left[\frac{1}{2}(\det A + \det B) - \det C\right]^2 - \det\sigma\right\}^{1/2}. \tag{30}$$

As in the previous section, for two-qubit ensembles a well-behaved steady-state solution of the Lindblad equation only exists for $\gamma \geqslant 1$. Thus, in the stationary regime ($t \to \infty$) the only nonzero entries of the covariance matrix in Eq. (24) are

$$\sigma_{xx} = \sigma_{yy} = \tfrac{1}{2}\cosh[2s(\Delta)] = \sigma_{p_x p_x} = \sigma_{p_y p_y}, \tag{31}$$

$$\sigma_{xy} = -\frac{1}{2\gamma}\sinh[2s(\Delta)] = -\sigma_{p_x p_y}, \tag{32}$$

yielding to the following close expression for the steady-state logarithmic negativity,

$$E_N^{ss} = \mathrm{Max}\left\{0, \log_2\left\{\frac{\gamma}{\gamma\cosh[2s(\Delta)] - \sinh[2s(\Delta)]}\right\}\right\}, \tag{33}$$

a result plotted in Fig. 6(a), where the borderline separating finite from zero E_N^{ss} regions (solid yellow line) is now given by

$$\sinh[2s(\Delta)] = \frac{2\gamma}{\gamma^2 - 1}. \tag{34}$$

An immediate comparison of this last result with that expressed by Eq. (23) for the two-qubit case leads us to conclude that the generation of steady-state entanglement between two-qubit ensembles is allowed in a wider region of the parameter space $[\gamma, s(\Delta)]$ than for a single-qubit pair. In other words, there are parameter points for which two-qubit steady-state entanglement never exists but, for the same parameter set, two-qubit ensembles can indeed get entangled. For selected points marked in Fig. 6(a) the ensembles entanglement evolution $E_N(t)$ is plotted in Fig. 6(b), where it can be seen that for any parameter set, $E_N(t) \sim t$ with a single time constant.

The behavior of E_N, both steady-state and time-dependent, as a function separately of the maximum microwave squeezing parameter s_0 and detuning Δ, for $\gamma = 1$, is shown in Fig. 7. Obviously, at resonance E_N^{ss} grows boundless as a function of s_0 [see Fig. 7(a)], however, with a fast degrading as the resonance condition is lost. For the time-dependent behavior, we found a single time-entanglement generation for any resonance detuning [see Figs. 7(b)–7(c)].

Entanglement generation results for dissipation rates outside the special line $\gamma = 1$ in Fig. 6(a) show a similar behavior as that reported in Sec. III for a qubit pair. Again notice that by increasing the detuning Δ one can cross the yellow line in Fig. 6(a), from above to below, allowing the qubit ensembles to become entangled at nonresonance conditions as shown in Figs. 8(a) and 8(b).

V. THERMAL DECOHERENCE EFFECTS

The open quantum aspects of the results discussed so far have been limited to the TLSMF entangled reservoirs action upon the matter systems. However, the matter qubits in realistic solid-state setups are also exposed to other interactions with different degrees of freedom within the material or with additional external radiation fields which yield to a matter entanglement decreasing, though the rate of the entanglement generation by the TLSMF reservoirs themselves remain unaltered. Therefore, it is necessary to quantify the effects of realistic decoherence processes in the present systems of interest: NV centers, magnetic molecules, and superconducting qubits. We concentrate on amplitude damping processes associated with thermal excitations as they constitute the main source of quantum correlation losses in

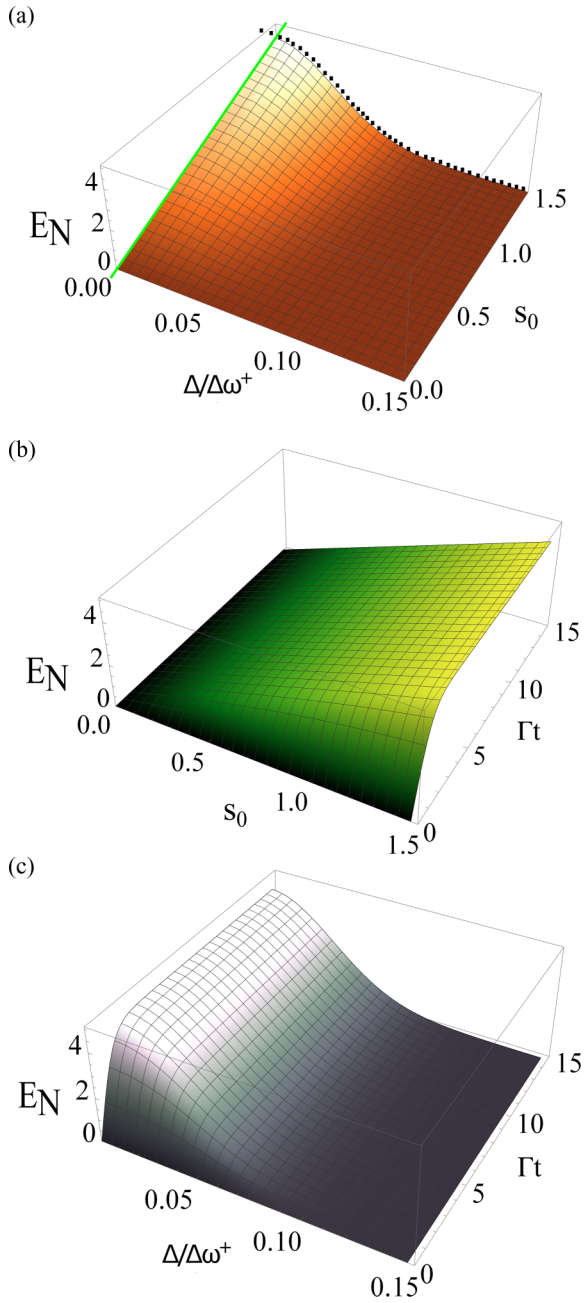

FIG. 7. Logarithmic negativity for two initially uncoupled qubit ensembles for $\gamma = 1$. (a) Steady-state E_N^{ss} as a function of the maximum squeezing strength s_0 and the central microwave frequency-qubit detuning, Δ. (b) Time-dependent $E_N(t)$ at resonance, $\Delta = 0$ [green points in (a)]. (c) Time-dependent $E_N(t)$ at fixed maximum squeezing $s_0 = 1.5$ [black points in (a)].

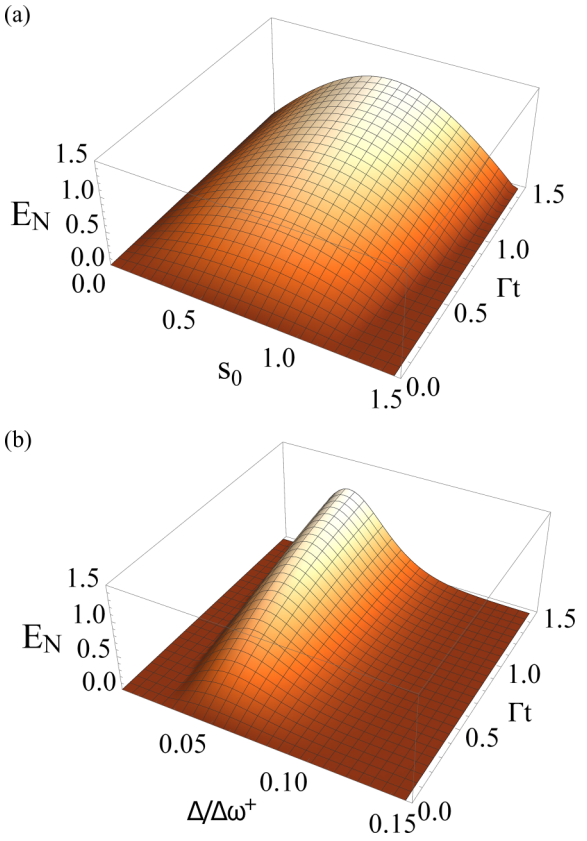

FIG. 8. Time-dependent logarithmic negativity, $E_N(t)$, for initially unentangled qubit ensembles with symmetric local dissipation rates larger than the cross-dissipation rate, $\gamma = 1.1$. (a) Resonance, $\Delta = 0$; (b) fixed maximum squeezing parameter $s_0 = 1.5$.

condensed-matter qubit systems [54]. However, if we focus on a specific solid-state realization a more detailed decoherence modeling might be required. Neighboring spins for NV centers [55], thermal fluctuations of dipolar interactions for magnetic molecules [56], and changes in the magnetic flux or external currents for superconducting qubits [57] are some particular examples of decoherence processes in different condensed-matter systems. If we include the thermal excitations, the full master equation takes the form

$$\frac{d\hat{\rho}}{dt} = \hat{\mathcal{L}}_{MW}\hat{\rho}(t) + \hat{\mathcal{L}}_D\hat{\rho}(t), \tag{35}$$

where $\hat{\mathcal{L}}_{MW}$ is given by Eqs. (16)–(19) and $\hat{\mathcal{L}}_D$ in Eq. (35) represents the decoherence Lindbladian term associated with amplitude or thermal damping processes as given by

$$\begin{aligned}\hat{\mathcal{L}}_D\hat{\rho}(t) = \sum_{j=1,2} \Gamma_j^{\text{th}}\{&(n_j+1)[2\hat{q}_j^-\hat{\rho}(t)\hat{q}_j^+ - \hat{q}_j^+\hat{q}_j^-\hat{\rho}(t) \\ &- \hat{\rho}(t)\hat{q}_j^+\hat{q}_j^-] + n_j[2\hat{q}_j^+\hat{\rho}(t)\hat{q}_j^- - \hat{q}_j^-\hat{q}_j^+\hat{\rho}(t) \\ &- \hat{\rho}(t)\hat{q}_j^-\hat{q}_j^+]\},\end{aligned} \tag{36}$$

where $n_j = (e^{\frac{\omega_j}{K_B T_j}} - 1)^{-1}$ denotes the Bose-Einstein occupation number for frequency ω_j of a thermal bath at temperature T_j (K_B is the Boltzmann constant) and Γ_j^{th} represents a Weisskopf-Wigner effective thermal decay rate, for each $j = 1,2$ matter subsystem. Notice that the decoherence/thermal Lindbladian $\hat{\mathcal{L}}_D$ in Eq. (36) has the same structure as the sum of local Lindbladians for the TLSMF case as given by Eq. (17). Thus, we can conclude that the presence of incoherent thermal processes affecting the spin-qubit systems will leave unaffected the nonlocal entangling TLSMF Lindblad term in Eq. (19). However, a stronger competition between entangling and nonentangling terms is now expected.

We concentrate upon discussing decoherence effects just for the steady-state entanglement behavior. For the two separate qubit case the borderline separating the entangled from unentangled steady-state regions can now be written as ($\Gamma_1^{\rm th} = \Gamma_2^{\rm th} = \Gamma^{\rm th}$ and $n_1 = n_2 = n$),

$$\sum_{i=0}^{6} p_i(\gamma,\gamma_{\rm th},n)x^i = 0, \tag{37}$$

with $x = \exp\{2s(\Delta)\}$ and $\gamma_{\rm th} = \Gamma^{\rm th}/\Gamma_{1,2}$. The explicit forms of functions $p_i(\gamma,\gamma_{\rm th},n)$ are given in Appendix B, where it is easily confirmed that in case of $\gamma_{\rm th} = 0$ it follows that $p_1 = p_3 = p_5 = 0$, retrieving the expression previously given in Eq. (23). For qubit ensembles in the presence of thermal effects the region in the $s(\Delta) - \gamma$ parameter plane of finite steady-state logarithmic negativity, E_N, is now given by the following inequalities:

$$p_-(\gamma,\gamma_{\rm th},n) \leqslant \exp\{s(\Delta)\} \leqslant p_+(\gamma,\gamma_{\rm th},n), \tag{38}$$

with

$$p_\pm(\gamma,\gamma_{\rm th},n) = \sqrt{\frac{\gamma - 2n\gamma_{\rm th} \pm \sqrt{1+4n\gamma_{\rm th}(n\gamma_{\rm th}-\gamma)}}{\gamma-1}}. \tag{39}$$

Notice that when $n\gamma_{\rm th} \to 0$ the borderline separating entangled from unentangled zones is given by

$$\exp\{s(\Delta)\} = \sqrt{\frac{\gamma+1}{\gamma-1}}, \tag{40}$$

which yields directly to Eq. (34).

Thermal decoherence effects on the TLSMF mediated entanglement generation for both cases, a qubit pair and multiqubit ensembles, are depicted in Figs. 9(a) and 9(b) for $\gamma_{\rm th} = 0.7$ and $n = 0.1$. First, by comparing the color scales in Figs. 9(a) and 9(b) with the corresponding scales in Figs. 3 and 6, we find that the maximum entanglement amount is reduced roughly one order of magnitude with respect to the pure TLSMF case. Second, a reduction of the entanglement zone when thermal effects are incorporated is also observed in both cases [the solid yellow lines correspond to the borderline separating the steady-state entangled-unentangled regions in the $s(\Delta) - \gamma$ parameter plane]. For the sake of comparison we also display with dashed yellow lines the $\gamma_{\rm th} = 0$ results as previously plotted in Figs. 3(a) and 6(a). For additional information we also plot, as white dotted lines, in Figs. 9(a) and 9(b) the borders of the steady-state finite entanglement regions for a higher-temperature situation, i.e., $\gamma_{\rm th} = 0.7$ and $n = 0.16$. Notice that for low microwave squeezing values, small $s(\Delta)$, the steady-state entanglement disappears quickly as the crossed squeezing term $\Gamma_{1,2}$ in Eq. (20) decreases or, equivalently, when γ values increase. Furthermore, it is evident that thermal decoherence effects impose, as a requirement for generating steady-state entanglement, a minimum amount of microwave squeezing $s(\Delta)$. Notice also that a maximum value of γ (or equivalently a minimum value of cross TLSMF rate $\Gamma_{1,2}$) as determined by each temperature, is required to achieve steady-state entanglement. These extreme values $[s^*(\Delta),\gamma^*]$ are represented in Fig. 9 with solid circles for qubit pairs and open circles for qubit ensembles. The dependence of these extreme values for a range of temperatures is depicted in Fig. 10, where the area of the circles is proportional to the average number of excitations n. Evidently, the larger the temperature a higher minimum value of cross TLSMF $\Gamma_{1,2}$ is required. The maximum value of concurrence for a qubit pair as a function of temperature (n) is shown in the inset of Fig. 10. Since the logarithmic negativity for the multiqubit systems is not bounded, a similar graph cannot be built for different temperatures. By including other sources of dissipation the long-time entanglement is further degraded; nevertheless, the qualitative behavior described previously is still observed. The optimal values of $\Gamma_{1,2}$ and $s(\Delta)$ can be controlled to reach a significant amount of entanglement.

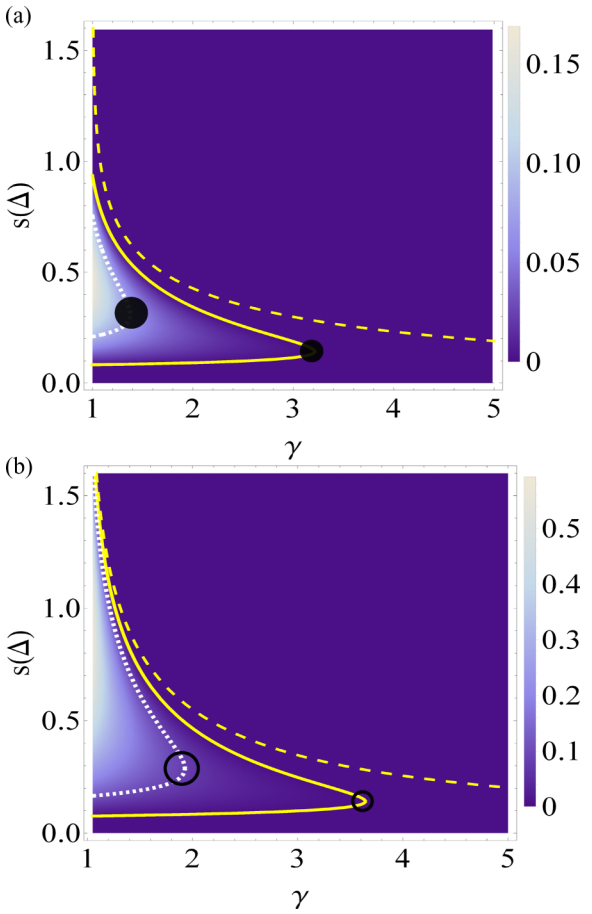

FIG. 9. Steady-state entanglement in the TLSMF parameter space $\{s(\Delta),\gamma\}$: (a) two-qubit concurrence C^{ss} and (b) two multispin logarithmic negativity, E_N^{ss}. For panels (a) and (b) lines represent the border separating entangled from unentangled states: dashed (yellow) lines denote pure TLSMF entanglement transfer, i.e., $\gamma_{\rm th} = 0.0$; solid (yellow) lines correspond to thermal coupling $\gamma_{\rm th} = 0.7$ and mean thermal excitation number $n = 0.1$, while dotted (white) lines denote a higher-temperature case with $\gamma_{\rm th} = 0.7$ and $n = 0.16$. Circles in the figures, with coordinates $\{s^*(\Delta),\gamma^*\}$, represent the maximum γ values, and corresponding squeezing $s(\Delta)$, to reach entangled states (see also Fig. 10).

All the main results described for the $\gamma_{\rm th} = 0$ situation survive well if decoherence towards thermal environments is on the same order of magnitude as the cross TLSMF $\Gamma_{1,2}$ value and low-enough temperatures. According to these results we conclude that thermal decoherence effects limit both the

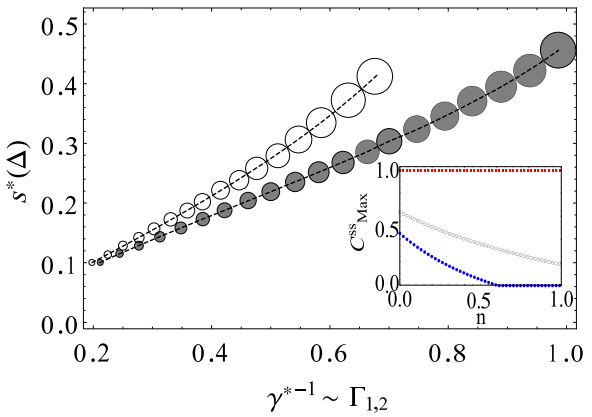

FIG. 10. Extreme values $s^*(\Delta)$ and $\gamma^{*-1} \sim \Gamma_{1,2}$ (see also Fig. 9) to obtain stationary entangled states for qubit pairs (solid circles) and qubit ensembles (open circles) for a thermal coupling $\gamma_{th} = 0.7$ as the temperature is varied, producing mean excitation thermal numbers ranging from $n = 0.05$ to $n = 0.19$. The area of each circle is proportional to n. (Inset) Maxima of steady-state concurrence for a qubit pair system as a function of n (or temperature): red squares represent no thermal bath $\gamma_{th} = 0$, open black circles $\gamma_{th} = 0.1$, and solid blue circles $\gamma_{th} = 0.3$

maximum amount of entanglement for the two cases considered as wells as the region in the $s(\Delta) - \gamma$ parameter space where a stationary entanglement can be reached. However, the existence of finite steady-state entanglement generated by TLSMF can survive the attack of thermal effects. Therefore, the entanglement transfer from entangled microwaves to solid-state qubits pairs or multiqubit ensembles is a reliable and robust process even in the presence of noisy environments.

VI. EXPERIMENTAL IMPLEMENTATION

We have explained two theoretical protocols to transfer quantum correlations from a squeezed bath to two initially uncoupled systems, either qubits or ensembles that behave like effective harmonic oscillators. We now discuss how these ideas can be adapted to a setup where the entangling bath is squeezed microwave radiation generated and propagating through a superconducting device.

JPAs [43] are superconducting devices that, by combining an external driving with some incoming radiation, can produce huge signal gains with the addition of very minimal, quantum limited noise. At the same time that they amplify the radiation, these devices are also capable of producing very large amounts of squeezing, either on some income field or in pure vacuum. From early implementations with about 50% noise reduction [58,59], state-of-the-art implementations now reach values of 10 dB squeezing in an input vacuum state [60], figures that improve every year. When operated in the frequency downconversion regime, JPA generates pairs of correlated photons in a two-mode squeezed state such as the one used in this work [22]. Alternatively to ordinary JPAs, we also find other Josephson devices in the literature which are specifically tuned for two-mode squeezing generation and which hold a greater potential for large squeezing values [24,26], already facilitating values of 12-dB two-mode squeezing [26].

Let us first discuss the situation in which the TLSMF couples to an ensemble of NV centers. The advantage of using spin ensembles composed by NV centers is the similar energy with the squeezed microwaves generated in quantum circuits. Each NV center has a $S = 1$ ground state, with zero-field splitting $\Delta = 2\pi \times 2.87$ GHz between the $m_s = 0$ and the $m_s = \pm 1$ states. By the application of an external magnetic field, one can isolate two spin transitions of this triplet due to the fact that the zero-field spin splitting Δ sets a preferred axis of quantization to be along the axis of the nitrogen-vacancy bond and model the NV like two qubits. For the coupling between the NV spin ensemble and the microwave field we have taken experimental reported parameters where for $N = 3 \times 10^7$ color centers $g \approx 2\pi \times 35$ MHz [29]. In order to quantify the entanglement between the ensembles once they have interacted with the correlated baths, we calculated the logarithmic negativity in Sec. IV and we show the optimal parameter of squeezing of the microwaves s_0 required. In Figs. 6 to 8 we can note that appreciable entanglement is obtained for $s_0 \leqslant 0.5$ in both regimes, time depending and stationary. This value corresponds to a gain $G_E = \cosh^2[s_0] = 1.27$ dB; therefore, the required squeezing for the microwaves to obtain maximum entangled values is in the range of the reported experimental values. The other essential parameter in that process is the Γ, where $\Gamma \sim g^2$. For the case of a spin ensemble, $g \approx 2\pi \times 35$ MHz, and the results show that with this parameter we can obtain significant values of entanglement between the two spin ensembles. In the stationary regime the E_N^{ss} function reaches the value 5 for $s_0 = 1.5$. The other experimental setup that we propose consists of two single qubits which are spatially separated and coupled to different transmission line modes. As we have seen above, a good qubit-radiation coupling is essential for a successful transfer of correlations, which may condition the implementation. If those qubits are NV centers, the typical coupling to the microwaves will be rather small, about 100 Hz for a bare line, or slightly larger, ~ 0.1 MHz, for more sophisticated coupling mechanisms [61,62], but always on the borderline and dominated by other dephasing or dissipation mechanisms. One interesting alternative is to rely on molecular magnets: Still in the range of microwaves, these macromolecules host ions with large magnetic moments and they can be placed cleverly for enhanced coupling with the radiation. For example, for molecules of Fe_8 the relation g/ω is three orders of magnitude greater than for NV centers [44]. Finally, the simplest route would be to use our protocol to entangle ordinary superconducting qubits. In QED circuit experiments strong coupling of microwave photons confined in a transmission line cavity with single superconducting qubits has already been demonstrated, with coupling strengths between matter and radiation reaching values of up to $g = 105$ MHz [63], while thermal decay effects in such low-temperature setups are so weak that effects in such low-temperature setups are so weak that our results shown in Figs. 9 and 10 are indeed relevant.

VII. CONCLUSIONS

Summing up, in this work we have proposed a hybrid system in order to study the dynamics of quantum correlations transferred to initially uncoupled single or spin ensembles

from a squeezed microwave field generated by JPA devices combining recent advances on parametric amplifiers with NV centers and other solid-state spin systems which share similar energy scales to that of controlled microwave radiation fields. For the case of spin ensembles we evidence a notable value for the entanglement without requiring high values for the squeezing parameter of microwaves r; this facilitates the possible experimental implementation. Even more interesting is the possibility of getting entanglement even in the stationary regimen. The experimental values for coupling between spin ensembles and microwaves show that this proposal would serve for obtain highly entangled states. In the case of the qubits it is of great interest to control single quantum particles and reach entanglement among them. The results show that if we combine the squeezed microwaves with single-molecule magnets or superconducting qubits it is possible to reach non-negligible spin entanglement values. We have established the robustness of TLSMF entanglement transfer processes under thermal dissipative conditions.

ACKNOWLEDGMENTS

A.V.G., F.J.R., and L.Q. acknowledge financial support from Facultad de Ciencias at UniAndes-2015 Project "Transfer of Correlations from Non-classically Correlated Reservoirs to Solid State Systems" and Project "Quantum Control of Non-equilibrium Hybrid Systems-Part II," UniAndes-2015. J.J.G.R. acknowledges support from Spanish Mineco Project No. FIS2012-33022, from EU FP7 Project PROMISCE, from CAM Research Network QUITEMAD+.

APPENDIX A: BROADBAND SQUEEZING TRANSFORMATIONS

To proceed further, it is important to realize that reservoir boson operators are transformed by the action of the squeezing operator $\hat{S}$ [see Eq. (7)] as

$$\begin{aligned}\hat{S}^{\dagger}\hat{a}_{n,j}\hat{S} &= \sum_{m}\left[A^{(1)}_{n,m}\hat{a}_{m,j} + A^{(2)}_{n,m}\hat{a}^{\dagger}_{m,\bar{j}}\right],\\ \hat{S}^{\dagger}\hat{a}^{\dagger}_{n,\bar{j}}\hat{S} &= \sum_{m}\left[A^{(1)}_{n,m}\hat{a}^{\dagger}_{m,\bar{j}} + A^{(2)}_{n,m}\hat{a}_{m,j}\right],\end{aligned} \tag{A1}$$

$j,\bar{j} = 1,2$, with $j+\bar{j}=3$. In Eq. (A1) the expressions for $A^{(j)}_{n,m}$ are given by

$$\begin{aligned}A^{(1)}_{n,m} &= \delta_{n,m} + \frac{1}{2!}\sum_{p} r_{n,p}r_{m,p}\\ &\quad + \frac{1}{4!}\sum_{p,q,r} r_{n,p}r_{q,p}r_{q,r}r_{m,r} + \cdots,\\ A^{(2)}_{n,m} &= r_{n,m} + \frac{1}{3!}\sum_{p,q} r_{n,p}r_{q,p}r_{q,m}\\ &\quad + \frac{1}{5!}\sum_{p,q,r,s} r_{n,p}r_{q,p}r_{q,r}r_{s,r}R_{s,m} + \cdots.\end{aligned} \tag{A2}$$

On inserting Eqs. (A1) into Eq. (12) it follows that the only different-from-zero partial traces over the reservoir degrees of freedom correspond to

$$\begin{aligned}\langle\hat{a}^{\dagger}_{n,1}\hat{a}_{m,1}\rangle &= \langle\hat{a}^{\dagger}_{n,2}\hat{a}_{m,2}\rangle = \sum_{p} A^{(2)}_{n,p}A^{(2)}_{m,p},\\ \langle\hat{a}^{\dagger}_{n,1}\hat{a}^{\dagger}_{m,2}\rangle &= \langle\hat{a}_{n,1}\hat{a}_{m,2}\rangle = \sum_{p} A^{(1)}_{n,p}A^{(2)}_{m,p},\\ \langle\hat{a}_{n,1}\hat{a}^{\dagger}_{m,1}\rangle &= \langle\hat{a}_{n,2}\hat{a}^{\dagger}_{m,2}\rangle = \sum_{p} A^{(1)}_{n,p}A^{(1)}_{m,p}.\end{aligned} \tag{A3}$$

On inserting Eq. (14), valid for a perfect correlated two-bath system, into Eq. (A2), we arrive to the simple expressions

$$\begin{aligned}A^{(1)}_{n,m} &= \delta_{n,m}\cosh(r_n),\\ A^{(2)}_{n,m} &= \delta_{n,m}\sinh(r_n).\end{aligned} \tag{A4}$$

On substituting Eqs. (A4) into Eqs. (A1) we obtain Eqs. (15).

APPENDIX B: COMPETITION BETWEEN SQUEEZING AND THERMAL EFFECTS

Here we proceed to give the explicit form for the steady-state two-qubit concurrence C^{ss}. It is given by

$$C^{ss} = \frac{1}{4}\frac{\sum_{i=0}^{6} p_i(\gamma,\gamma_{\rm th},n)x^i}{\sum_{i=0}^{6} q_i(\gamma,\gamma_{\rm th},n)x^i}, \tag{B1}$$

with $x = \exp\{2s(\Delta)\}$ and the explicit forms of functions $p_i(\gamma,\gamma_{\rm th},n)$ and $q_i(\gamma,\gamma_{\rm th},n)$ are

$$\begin{aligned}p_0(\gamma,\gamma_{\rm th},n) &= p_6(\gamma,\gamma_{\rm th},n) = -\gamma(\gamma^2-1),\\ p_1(\gamma,\gamma_{\rm th},n) &= p_5(\gamma,\gamma_{\rm th},n) = 2\gamma_{\rm th}(1+2n)(1-3\gamma^2),\\ p_2(\gamma,\gamma_{\rm th},n) &= -\gamma - 8\gamma^2 + \gamma^3 - 16\gamma\gamma_{\rm th} + 8\gamma^2\gamma_{\rm th} - 8\gamma_{\rm th}^2\\ &\quad - 8\gamma\gamma_{\rm th}^2 - 48\gamma\gamma_{\rm th}^2 n(n+1),\\ p_4(\gamma,\gamma_{\rm th},n) &= -\gamma + 8\gamma^2 + \gamma^3 + 16\gamma\gamma_{\rm th} + 8\gamma^2\gamma_{\rm th}\\ &\quad + 8\gamma_{\rm th}^2 - 8\gamma\gamma_{\rm th}^2 - 48\gamma\gamma_{\rm th}^2 n(n+1),\\ p_3(\gamma,\gamma_{\rm th},n) &= -4\gamma_{\rm th}[1+\gamma^2-4\gamma\gamma_{\rm th}+2(1+\gamma^2)n\\ &\quad - 8\gamma_{\rm th}n(\gamma_{\rm th}-\gamma+3\gamma_{\rm th}n+2\gamma_{\rm th}n^2)],\end{aligned} \tag{B2}$$

and

$$\begin{aligned}q_0(\gamma,\gamma_{\rm th},n) &= q_6(\gamma,\gamma_{\rm th},n) = \gamma(\gamma^2-1),\\ q_1(\gamma,\gamma_{\rm th},n) &= q_5(\gamma,\gamma_{\rm th},n) = \gamma[1+3\gamma^2+12\gamma_{\rm th}^2(1+2n)^2],\\ q_2(\gamma,\gamma_{\rm th},n) &= q_4(\gamma,\gamma_{\rm th},n) = -\gamma - 8\gamma^2 + \gamma^3 - 16\gamma\gamma_{\rm th}\\ &\quad + 8\gamma^2\gamma_{\rm th} - 8\gamma_{\rm th}^2 - 8\gamma\gamma_{\rm th}^2 - 48\gamma\gamma_{\rm th}^2 n(n+1),\\ q_3(\gamma,\gamma_{\rm th},n) &= 16\gamma_{\rm th}[(1+2n)(1+3\gamma^2) + 2\gamma_{\rm th}^2(1+6n\\ &\quad + 12n^2 + 8n^3)].\end{aligned} \tag{B3}$$

[1] A. K. Ekert, Phys. Rev. Lett. **67**, 661 (1991).

[2] N. Gisin, G. Ribordy, W. Tittel, and H. Zbinden, Rev. Mod. Phys. **74**, 145 (2002).

[3] C. H. Bennett, G. Brassard, C. Crépeau, R. Jozsa, A. Peres, and W. K. Wootters, Phys. Rev. Lett. **70**, 1895 (1993).

[4] H. J. Briegel, D. E. Browne, W. Dür, R. Raussendorf, and M. Van den Nest, Nat. Phys. **5**, 19 (2009).

[5] R. Raussendorf and H. J. Briegel, Phys. Rev. Lett. **86**, 5188 (2001).

[6] I. L. Chuang and D. Gottesman, Nature (London) **402**, 390 (1999).

[7] Q. A. Turchette, C. S. Wood, B. E. King, C. J. Myatt, D. Leibfried, W. M. Itano, C. Monroe, and D. J. Wineland, Phys. Rev. Lett. **81**, 3631 (1998).

[8] D. L. Moehring, P. Maunz, S. Olmschenk, K. C. Younge, D. N. Matsukevich, L.-M. Duan, and C. Monroe, Nature (London) **449**, 68 (2007).

[9] F. Schmidt-Kaler, H. Häffner, M. Riebe, S. Gulde, G. P. T. Lancaster, T. Deuschle, C. Becher, C. F. Roos, J. Eschner, and R. Blatt, Nature (London) **422**, 408 (2003).

[10] B. Julsgaard, A. Kozhekin, and E. S. Polzik, Nature (London) **413**, 400 (2001).

[11] C. W. Chou, H. de Riedmatten, D. Felinto, S. V. Polyakov, S. J. van Enk, and H. J. Kimble, Nature (London) **438**, 828 (2005).

[12] D. N. Matsukevich, T. Chanelière, S. D. Jenkins, S.-Y. Lan, T. A. B. Kennedy, and A. Kuzmich, Phys. Rev. Lett. **96**, 030405 (2006).

[13] M. Schug, J. Huwer, C. Kurz, P. Müller, and J. Eschner, Phys. Rev. Lett. **110**, 213603 (2013).

[14] W. B. Gao, P. Fallahi, E. Togan, J. Miguel-Sanchez, and A. Imamoglu, Nature (London) **491**, 426 (2012).

[15] P. Neumann, R. Kolesov, B. Naydenov, J. Beck, F. Rempp, M. Steiner, V. Jacques, G. Balasubramanian, M. L. Markham, D. J. Twitchen, S. Pezzagna, J. Meijer, J. Twamley, F. Jelezko, and J. Wrachtrup, Nat. Phys. **6**, 249 (2010).

[16] H. Bernien, B. Hensen, W. Pfaff, G. Koolstra, M. S. Blok, L. Robledo, T. H. Taminiau, M. Markham, D. J. Twitchen, L. Childress, and R. Hanson, Nature (London) **497**, 86 (2013).

[17] B. Hensen, H. Bernien, A. E. Drèau, A. Reiserer, N. Kalb, M. S. Blok, J. Ruitenberg, R. F. L. Vermeulen, R. N. Schouten, C. Abellàn, W. Amaya, V. Pruneri, M. W. Mitchell, M. Markham, D. J. Twitchen, D. Elkouss, S. Wehner, T. H. Taminiau, and R. Hanson, Nature (London) **526**, 682 (2015).

[18] M. Ansmann, H. Wang, R. C. Bialczak, M. Hofheinz, E. Lucero, M. Neeley, A. D. OĆonnell, D. Sank, M. Weides, J. Wenner *et al.*, Nature (London) **461**, 504 (2009).

[19] J. M. Chow, L. DiCarlo, J. M. Gambetta, A. Nunnenkamp, L. S. Bishop, L. Frunzio, M. H. Devoret, S. M. Girvin, and R. J. Schoelkopf, Phys. Rev. A **81**, 062325 (2010).

[20] M. Baur, A. Fedorov, L. Steffen, S. Filipp, M. P. da Silva, and A. Wallraff, Phys. Rev. Lett. **108**, 040502 (2012).

[21] J. del Pino, J. Feist, F. J. García-Vidal, and J. J. García-Ripoll, Phys. Rev. Lett. **112**, 216805 (2014).

[22] C. Eichler, D. Bozyigit, C. Lang, M. Baur, L. Steffen, J. M. Fink, S. Filipp, and A. Wallraff, Phys. Rev. Lett. **107**, 113601 (2011).

[23] E. P. Menzel, R. Di Candia, F. Deppe, P. Eder, L. Zhong, M. Ihmig, M. Haeberlein, A. Baust, E. Hoffmann, D. Ballester, K. Inomata, T. Yamamoto, Y. Nakamura, E. Solano, A. Marx, and R. Gross, Phys. Rev. Lett. **109**, 250502 (2012).

[24] E. Flurin, N. Roch, F. Mallet, M. H. Devoret, and B. Huard, Phys. Rev. Lett. **109**, 183901 (2012).

[25] C. Lang, C. Eichler, L. Steffen, J. M. Fink, M. J. Woolley, A. Blais, and A. Wallraff, Nat. Phys. **9**, 345 (2013).

[26] C. Eichler, Y. Salathe, J. Mlynek, S. Schmidt, and A. Wallraff, Phys. Rev. Lett. **113**, 110502 (2014).

[27] Z.-L. Xiang, X.-Y. Lü, T.-F. Li, J. Q. You, and F. Nori, Phys. Rev. B **87**, 144516 (2013).

[28] D. Marcos, M. Wubs, J. M. Taylor, R. Aguado, M. D. Lukin, and A. S. Sørensen, Phys. Rev. Lett. **105**, 210501 (2010).

[29] X. Zhu, S. Saito, A. Kemp, K. Kakuyanagi, S.-i. Karimoto, H. Nakano, W. J. Munro, Y. Tokura, M. S. Everitt, K. Nemoto *et al.*, Nature (London) **478**, 221 (2011).

[30] Y. Kubo, C. Grezes, A. Dewes, T. Umeda, J. Isoya, H. Sumiya, N. Morishita, H. Abe, S. Onoda, T. Ohshima, V. Jacques, A. Dréau, J.-F. Roch, I. Diniz, A. Auffeves, D. Vion, D. Esteve, and P. Bertet, Phys. Rev. Lett. **107**, 220501 (2011).

[31] R. Amsüss, C. Koller, T. Nöbauer, S. Putz, S. Rotter, K. Sandner, S. Schneider, M. Schramböck, G. Steinhauser, H. Ritsch, J. Schmiedmayer, and J. Majer, Phys. Rev. Lett. **107**, 060502 (2011).

[32] D. I. Schuster, A. P. Sears, E. Ginossar, L. DiCarlo, L. Frunzio, J. J. L. Morton, H. Wu, G. A. D. Briggs, B. B. Buckley, D. D. Awschalom, and R. J. Schoelkopf, Phys. Rev. Lett. **105**, 140501 (2010).

[33] Y. Kubo, F. R. Ong, P. Bertet, D. Vion, V. Jacques, D. Zheng, A. Dréau, J.-F. Roch, A. Auffeves, F. Jelezko, J. Wrachtrup, M. F. Barthe, P. Bergonzo, and D. Esteve, Phys. Rev. Lett. **105**, 140502 (2010).

[34] Y. Kubo, I. Diniz, A. Dewes, V. Jacques, A. Dréau, J.-F. Roch, A. Auffeves, D. Vion, D. Esteve, and P. Bertet, Phys. Rev. A **85**, 012333 (2012).

[35] Y. Matsuzaki, X. Zhu, K. Kakuyanagi, H. Toida, T. Shimooka, N. Mizuochi, K. Nemoto, K. Semba, W. J. Munro, H. Yamaguchi, and S. Saito, Phys. Rev. A **91**, 042329 (2015).

[36] S. Felicetti, M. Sanz, L. Lamata, G. Romero, G. Johansson, P. Delsing, and E. Solano, Phys. Rev. Lett. **113**, 093602 (2014).

[37] B. Kraus and J. I. Cirac, Phys. Rev. Lett. **92**, 013602 (2004).

[38] M. Paternostro, G. Falci, M. Kim, and G. M. Palma, Phys. Rev. B **69**, 214502 (2004).

[39] G. Adesso, S. Campbell, F. Illuminati, and M. Paternostro, Phys. Rev. Lett. **104**, 240501 (2010).

[40] M. Paternostro, W. Son, and M. S. Kim, Phys. Rev. Lett. **92**, 197901 (2004).

[41] S. Zippilli and F. Illuminati, Phys. Rev. A **89**, 033803 (2014).

[42] S. Zippilli, M. Paternostro, G. Adesso, and F. Illuminati, Phys. Rev. Lett. **110**, 040503 (2013).

[43] B. Yurke, J. Opt. Soc. Am. B **4**, 1551 (1987).

[44] M. Jenkins, T. Hümmer, M. J. Martínez-Pérez, J. García-Ripoll, D. Zueco, and F. Luis, New J. Phys. **15**, 095007 (2013).

[45] L. Quiroga, F. J. Rodríguez, M. E. Ramírez, and R. París, Phys. Rev. A **75**, 032308 (2007).

[46] J. C. Castillo, F. J. Rodríguez, and L. Quiroga, Phys. Rev. A **88**, 022104 (2013).

[47] M. Scully and M. Zubairy, *Quantum Optics* (Cambridge University Press, Cambridge, UK, 1997).

[48] L. J. Salazar, D. A. Guzmán, F. J. Rodríguez, and L. Quiroga, Opt. Express **20**, 4470 (2012).

[49] J. Laurat, G. Keller, J. A. Oliveira-Huguenin, C. Fabre, T. Coudreau, A. Serafini, G. Adesso, and F. Illuminati, J. Opt. B **7**, S577 (2005).
[50] W. K. Wootters, Phys. Rev. Lett. **80**, 2245 (1998).
[51] T. Hümmer, G. M. Reuther, P. Hänggi, and D. Zueco, Phys. Rev. A **85**, 052320 (2012).
[52] G. Vidal and R. F. Werner, Phys. Rev. A **65**, 032314 (2002).
[53] A. Serafini, F. Illuminati, M. G. A. Paris, and S. De Siena, Phys. Rev. A **69**, 022318 (2004).
[54] A. Blais, R.-S. Huang, A. Wallraff, S. M. Girvin, and R. J. Schoelkopf, Phys. Rev. A **69**, 062320 (2004).
[55] G. de Lange, Z. H. Wang, D. Riste, V. V. Dobrovitski, and R. Hanson, Science **330**, 60 (2010).
[56] V. V. Dobrovitski, M. I. Katsnelson, and B. N. Harmon, Phys. Rev. Lett. **84**, 3458 (2000).
[57] F. Yoshihara, K. Harrabi, A. O. Niskanen, Y. Nakamura, and J. S. Tsai, Phys. Rev. Lett. **97**, 167001 (2006).
[58] B. Yurke, R. Movshovich, P. G. Kaminsky, A. D. Smith, A. H. Silver, R. W. Simon, M. V. Schneider, and R. Trambarulo, Phys. B (Amsterdam, Neth.) **169**, 432 (1991).
[59] B. Yurke, P. G. Kaminsky, R. E. Miller, E. A. Whittaker, A. D. Smith, A. H. Silver, and R. W. Simon, Phys. Rev. Lett. **60**, 764 (1988).
[60] M. A. Castellanos-Beltran, K. D. Irwin, G. C. Hilton, L. R. Vale, and K. W. Lehnert, Nat. Phys. **4**, 929 (2008).
[61] J. Twamley and S. D. Barrett, Phys. Rev. B **81**, 241202 (2010).
[62] M. Gao, C.-W. Wu, Z.-J. Deng, W.-J. Zou, L.-g. Zhou, C.-Z. Li, and X.-B. Wang, Phys. Lett. A **376**, 595 (2012).
[63] J. Majer, J. M. Chow, J. M. Gambetta, J. Koch, B. R. Johnson, J. A. Schreier, L. Frunzio, D. I. Schuster, A. A. Houck, A. Wallraff *et al.*, Nature (London) **449**, 443 (2007).